



PERGAMON

Aerosol Science 32 (2001) 583–599

Journal of
Aerosol Science

www.elsevier.com/locate/jaerosci

Space-charge effects in nanoparticle processing using the differential mobility analyzer

Renato P. Camata^{a,*}, Harry A. Atwater^a, Richard C. Flagan^b

^aThomas J. Watson Laboratory of Applied Physics, California Institute of Technology, Pasadena, CA 91125, USA

^bDivision of Chemistry and Chemical Engineering, California Institute of Technology, Pasadena, CA 91125, USA

Received 9 November 1999; received in revised form 21 August 2000; accepted 28 August 2000

Abstract

We report the observation of mobility classification breakdown due to strong space-charge effects during nanoparticle processing in a radial differential mobility analyzer (DMA). A simple dimensionless group, the space-charge number, is introduced to help identify the conditions for which this phenomenon becomes important. Our analysis suggests a few DMA design features and operation conditions that should enable the accurate classification of ultrafine aerosols with high concentrations of charged particles. © 2001 Elsevier Science Ltd. All rights reserved.

Keywords: Differential mobility analyzer; Charged particles; Space charge; Ultrafine aerosols

1. Introduction

The differential mobility analyzer (DMA) is the key instrument in the measurement of ultrafine aerosol particles (Flagan, 1998). It is used directly in most measurements of aerosols below 100-nm diameter, and indirectly as a calibration source for most of the other instruments used in this size regime.

The DMA was originally developed to classify submicron aerosols at relatively low concentrations ($< 10^5 \text{ cm}^{-3}$). Under these conditions, charged particle losses within the classification region of the DMA are small, and the instrument closely approximates the predicted ideal performance

* Corresponding author. Tel.: + 1-205-934-8143; fax: + 1-205-934-8042.

E-mail address: camata@uab.edu (R.P. Camata).

¹ Present address: Department of Physics, The University of Alabama at Birmingham, Birmingham, Alabama (35294-1170), USA.

(Knutson & Whitby, 1975). This nearly optimal behavior has been achieved for cylindrical DMAs of a number of designs (Knutson & Whitby, 1975; Winklmayr, Reischl, Lidner & Berner 1991; Chen & Pui, 1998), and for radial-flow instruments (Meshah, 1994; Zhang, Akutsu, Russell, Flagan & Seinfeld, 1995).

The classification capabilities of the DMA were first described using trajectory models that describe the migration of nondiffusive, i.e., large, particles through the instrument (Knutson & Whitby, 1975), even though those same authors recognized that diffusion could distort the measurements at small particle sizes. Later investigators developed numerical (Kousaka, Okuyama, Adachi, & Mimura, 1986) and semi-analytical (Stolzenburg, 1988; see also Zhang & Flagan, 1996) descriptions of DMA classification of diffusive particles. These theoretical developments allow increased confidence in DMA measurements of size distributions in the lower nanometer range.

Several investigators observed slight size biases when one DMA was used to calibrate another one. It was noted that space-charge effects caused by the cumulative effects of the electric fields of all of the particles in the classification region could distort DMA measurements, possibly contributing to the observed bias (Stolzenburg, 1988; Alonso & Kousaka, 1996), although calculations showed that the effect should be much smaller than the observed shift at typical environmental particle concentrations. Similar effects had previously been reported in mobility analyzers in which the aerosol containing charged particles fills the gap between the two electrodes of a capacitor (Tammet, 1970). Chen and Pui (1997) used two-dimensional flows and electric fields within the TSI-short DMA to show that local distortions near the aerosol entrance port accounted for most of the observed distortion. Subsequent refinements to the DMA entrance slot have drastically reduced the perturbation and validated those predictions (Eichler, de Juan & Fernández de la Mora, 1998; Chen, Pui, Mulholland & Fernandez, 1999).

Although space-charge effects are generally minor in measurement of environmental aerosols, new applications of the DMA involve such high particle concentrations that space-charge effects cannot be ignored. DMAs are now being used to sort aerosol particles with respect to size to generate deposits for study of size-dependent properties and fabrication of nanoparticle-based microelectronic and optical devices (Camata, Atwater, Vahala & Flagan, 1996; Magnusson, Deppert, Malm & Svensson, 1997; Kruis, Fissan & Peled, 1998a). To produce dense deposits in a reasonable time, high concentration aerosols must be processed through the DMA.

In this paper, we present evidence that space-charge effects can disturb the performance of the DMA to the point of causing a complete breakdown of mobility classification. In order to determine the conditions under which this phenomenon becomes significant, we introduce a space-charge number, a dimensionless group which provides an estimate of the intensity of the space-charge effect in the DMA. Our simple analysis suggests some design features that should be considered in tailoring the DMA for high-throughput nanoparticle processing and materials synthesis applications.

2. High-throughput size classification and materials synthesis

Materials synthesis from size-classified aerosol particles often calls for the deposition of the gas-borne particles on a substrate. Assuming unity collection efficiency and neglecting particle

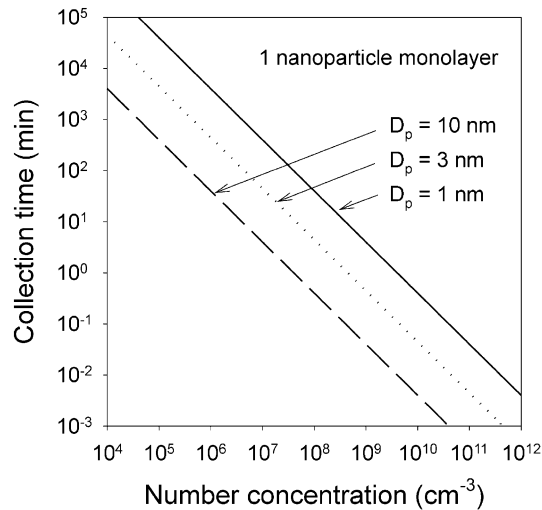


Fig. 1. Time required to deposit one nanoparticle monolayer as a function of number concentration for different particle diameters. Calculation for a nozzle-to-plane electrostatic precipitator with singly charged particles, aerosol flow rate of 1 SLM and deposit radius of 1 mm.

pile-up, the time t required to generate a uniform monolayer deposit of singly charged nanoparticles over an area A is given by

$$t = \frac{4A}{NQ\pi D_p^2}, \quad (1)$$

where D_p is the nanoparticle diameter, N is the particle number concentration and Q is the volumetric aerosol flow rate.

Fig. 1 shows this estimate of the deposition time for a 1-mm diameter circular deposit using an aerosol flow rate of 1 SLM (standard liter per minute). It is obvious that high aerosol concentrations are required to deposit usable amounts of size-classified nanoparticles. For typical aerosol concentrations of 10^4 cm^{-3} , several days would be required to deposit one monolayer of 10 nm particles. Deposits of smaller particles may demand weeks. Operation for such extended periods of time is usually impractical even for fully automated systems. High throughput and reasonable collection times could be achieved, however, if elevated number concentrations were processed in the DMA.

Ideally, one would like to perform size classification at concentrations in the 10^7 – 10^9 cm^{-3} range to generate deposits equivalent to several nanoparticle monolayers in a matter of hours or even minutes. Reliable operation in this regime would fully enable the DMA as a materials processing device.

3. Attempting mobility classification on highly charged aerosols

Two issues arise when one considers the use of the DMA at these high concentrations of charged particles. First, can these concentrations be achieved at all in the sub-10-nm size range? Second,

what is the maximum number concentration the DMA can process without significant distortion of the transfer function due to space-charge effects?

3.1. Aerosol generation and charging in the sub-10-nm size range

Although a detailed discussion of aerosol charging is beyond the scope of this paper, it must be said that much progress has been made in the charging of sub-10-nm aerosol particles. Chargers with extrinsic charging efficiency as high as 60% at 10 nm and 20% at 3 nm have been reported recently (Chen & Pui, 1998; Kruis, Otten, Jordan & Fissan, 1998b). However, the long residence times required by these devices to impart charge on the aerosol (>1 s) are sufficient to allow considerable coagulation, reducing the number concentration and producing agglomerates. Alternative approaches to particle charging are needed, therefore.

Another way to boost the number of charged particles is to employ methods of particle generation that inherently produce highly charged aerosols. One such example is aerosol generation by spark discharge. This method produces significant concentrations of charged ultrafine particles (Schwing, Garwin & Schmidt-Ott, 1988). Evidently, the problem of multiply charged particles comes into play, which makes this approach less than ideal. Nevertheless, if a significant number of particles can be obtained already charged, at least partial size classification at high throughput may be possible. Furthermore, improvements in such generation routes may allow some control of the aerosol charge state without the use of an additional charging device with long residence time.

In the measurements reported in this paper we have used spark discharge and thermal evaporation to generate aerosols with high number concentrations of charged silicon particles.

A schematic of the spark-discharge source used is shown in Fig. 2(a). A silicon aerosol is produced by ablation and evaporation of crystalline silicon substrates in a high-voltage electric spark discharge (Saunders et al., 1993; Camata et al., 1996). A flashlamp circuit (L , C , and R_1) is used to drive the discharge, while an additional resistor (R_2) limits the spark current to avoid

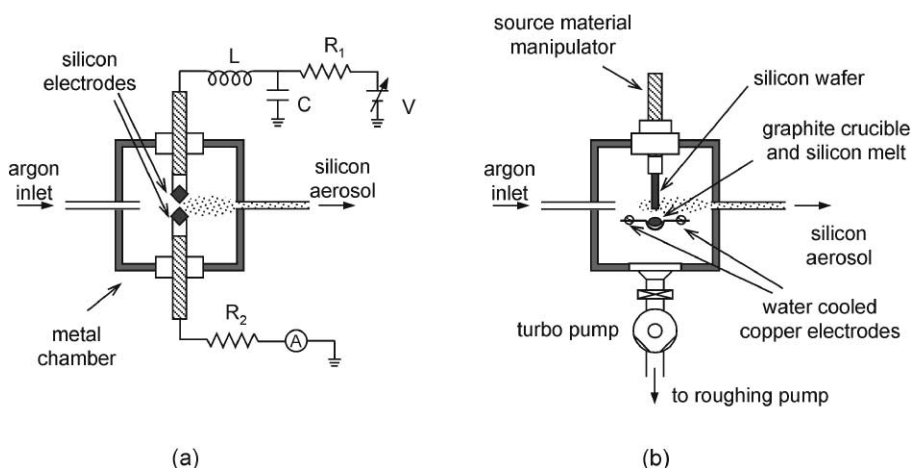


Fig. 2. Schematic of the spark discharge (a) and thermal evaporation (b) silicon aerosol sources used in this work.

excessive particle generation. The source is operated at 1-atm pressure while voltage, current, frequency and flow rate in the spark-discharge region are adjusted to generate an ultrafine aerosol in the 1–20 nm size range. The values used for the elements of the driving circuit are $R_1 = 10 \text{ k}\Omega$, $C = 0.125 \text{ }\mu\text{F}$ and $L = 70 \text{ }\mu\text{H}$. The spark current is best controlled by varying the resistance R_2 . Values between 0 and 200 k Ω have been used to vary the spark current in the 1–500 mA range. Typical voltage and frequency are 1 kV and 120 Hz, respectively. A volumetric flow rate of 1 SLM is usually used.

Another approach we have employed to generate a silicon aerosol with high concentration of charged particles was thermal evaporation (Dinh, Chase, Balooch, Siekhaus & Wooten, 1996). A schematic of the source used is depicted in Fig. 2(b). In this case, a 30–70 A AC electric current is run through a thin custom-made graphite crucible supported by water-cooled copper electrodes. The crucible design is such that high temperatures are reached only at the expected location of the melt. In this way the temperatures experienced by the copper electrodes are low enough that copper vaporization is negligible. At the central region of the crucible, resistive heating provides temperatures in excess of 1600°C. The crucible temperature was measured using a disappearing filament optical pyrometer. A silicon wafer suspended from a linear motion manipulator brings material into the hot surface of the crucible allowing melting to occur. Temperatures at the chamber walls reach $\sim 300^\circ\text{C}$, so a bake-out procedure is required before actual silicon evaporation. For this purpose a turbo-molecular pump was connected to the evaporation chamber through a valve. Before aerosol generation, the system is routinely out-gassed at normal operation conditions for about 12 h.

Both spark discharge and thermal evaporation can be used for aerosol generation over a wide range of experimental conditions. In both cases, particles are often obtained from the generation process already charged. This makes them reasonable alternatives as sources of aerosols with high concentration of charged particles required in applications of DMA nanoparticle processing. In the measurements reported in this paper, these two methods were observed to produce bipolar aerosols with positive net charge. The charging mechanisms involved have not been investigated in detail, and a thorough analysis is beyond the scope of this report. However, our observations allow us to make a few inferences about the processes of charged particle generation. In the case of the spark-discharge method, most of the evaporation takes place at the negative silicon electrode. This occurs as a result of bombardment by argon ions generated in the discharge, a fact that manifests itself by a visible plasma glow surrounding the negative electrode. Most particles are formed in this region of positively ionized plasma which is consistent with the generation of an aerosol with net positive charge. In the thermal evaporation source, the high temperatures used for silicon vaporization (1500–1600°C) are expected to induce thermal ionization processes. Although the details of thermal charging of nanoparticles are not yet fully understood, this phenomenon has been reported recently by Magnusson, Deppert and Krinke (1998) and a process involving electron emission is the most likely candidate for particle charging.

Regardless of the possible charging mechanisms, it must be emphasized that little is known about the relative concentrations of different charge states in the aerosol produced by spark discharge and thermal evaporation. Multiply charged particles are expected to play an important if not the dominant role in the electrical behavior of the product aerosols. Detailed investigations in this area are needed to accurately assess the potential of these techniques as controlled sources of charged nanoparticles. Nevertheless, it has been our observation that, under proper conditions,

both approaches allow the generation of charged sub-10-nm particles in concentrations significantly higher than obtained with conventional chargers.

3.2. Maximum number concentration of charged particles in the DMA

The second question associated with the use of the DMA as a processing device relates to the concentration of charged particles it can process without significant distortion of the transfer function. This is the main focus of this paper.

Fig. 3 shows a schematic of the experimental setup we have used to attempt the mobility classification of highly charged aerosols. Argon gas is supplied to a metallic cell where spark discharge or thermal evaporation was used to generate an aerosol of silicon nanoparticles. The polydisperse aerosol is introduced into a radial DMA (RDMA: Zhang et al., 1995) for mobility classification either directly from the source, or after passing through a ^{85}Kr neutralizer. The classified particles are then deposited on a substrate by hypersonic impactation (Fernández de la Mora, Hering, Rao & McMurry, 1990) for transmission electron microscopy (TEM) analysis. The apparatus is also equipped with an electrometer to probe the total charge carried by the aerosol at different points in the flow system. Our first experiment was run using the spark discharge aerosol source with an argon flow rate of 1 SLM. Using $R_2 = 10 \text{ k}\Omega$ and $V = 1.8 \text{ kV}$, an average spark current of 82 mA is obtained. Under these conditions, the negative silicon electrode is observed to melt taking the shape of what appears to be a solid droplet. After this transient melting behavior, RDMA measurements on particles that have passed through the neutralizer yield an approximately log-normal size distribution with $\bar{D}_{\text{pg}} \approx 20 \text{ nm}$, $\sigma_g = 1.47$ and total number concentration around 10^8 cm^{-3} . The current measurements that lead to this distribution are stable over several hours of operation, ensuring the reproducibility of the results reported here. In Fig. 4 we show how the electrometer current changes as aerosol is drawn from different points of the experiment. This serves as a qualitative indication of variations of the aerosol charge state along the experimental setup.

Upstream of the source (position 1), no particles are present, so the electrometer current is zero. Immediately downstream of the source (position 2), an aerosol with positive net charge is detected.

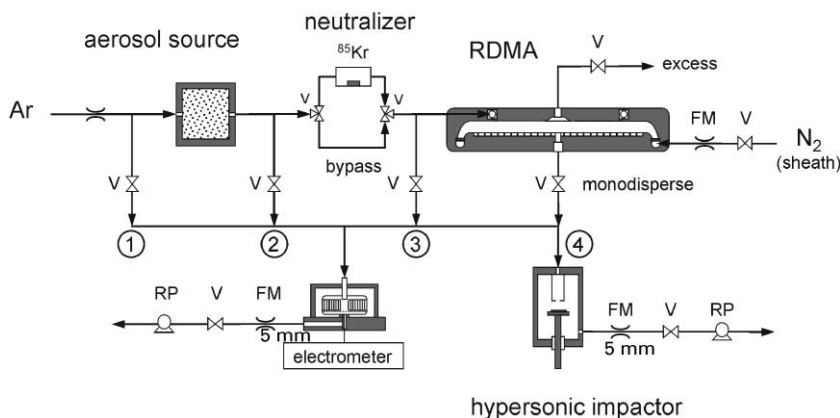


Fig. 3. Experimental setup used to attempt the mobility classification of highly charged aerosols. In the figure FM, V, and RP stand for flow meter, valve, and rotary pump, respectively.

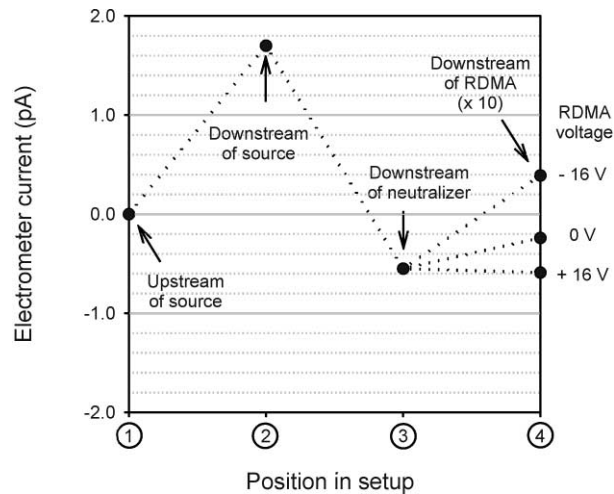


Fig. 4. Measurements of the aerosol net charge at different positions in an experiment using the spark-discharge source.

This is consistent with the notion that the particles are formed in the positively ionized plasma surrounding the negative silicon electrode where most of the evaporation takes place. Once the particles are run through the neutralizer (position 3) the population acquires a net negative charge. This is a common occurrence in equilibrium charging processes caused by the higher mobility of the negative ions with respect to the positive ones (see, for example, Adachi, Kousaka & Okuyama, 1985). At the RDMA classified aerosol outlet (position 4) the application of voltages of opposite polarities (± 16 V) draws particles of opposite signs, as it should be expected from our bipolar aerosol. We have observed, however, that an aerosol with negative net charge is still transmitted through the instrument when the voltage applied to the RDMA is zero. As we have ensured operation in the laminar regime with balanced flows, two processes could be responsible for this phenomenon, namely, diffusion and space-charge effects. Diffusion seems an unlikely explanation since the electrode separation in the RDMA (1 cm) far exceeds the root mean square distance traveled by the particles due to diffusion. We know from systematic studies of the spark-discharge aerosol using our setup with the electrometer as well as with a condensation nucleus counter (Camata et al., 1996), that its time evolution is dominated by coagulation as the particles travel from the source to the RDMA. This travel time is ~ 10 s. Repeated mobility and TEM measurements indicate that for this travel time and the spark currents used here, broad log-normal size distributions with $\bar{D}_{pg} \approx 20$ nm, $\sigma_g = 1.47$ and total number concentration around 10^8 cm $^{-3}$ are produced. For this kind of size distribution and the residence time of the RDMA ($t = 0.43$ s), the number of particles expected to reach the sampling port by diffusion alone is negligible. Thus, the space-charge effect appears to be the most reasonable explanation for this phenomenon. The field of the particles themselves might be driving small particles across the sheath flow and into the monodisperse outlet.

Knowledge of the net charge of the aerosol that enters the RDMA should provide an estimate of the magnitude of the space-charge field inside the instrument. Unfortunately, however, the electrometer is known to perform poorly at high concentrations of charged particles due to the very

space-charge field we are attempting to probe (Yun, Otani & Emi, 1997). Thus, the measurements displayed in Fig. 4 can only be interpreted qualitatively as the electrometer may significantly underestimate the charge state of the aerosol.

Spark discharge is a process that inherently produces highly charged aerosols. In order to see whether particle transmission through the DMA at zero voltage could also be observed when a thermal evaporation aerosol was used, we have run a second experiment employing the thermal evaporation source. Fig. 5 shows data obtained for silicon particles generated by thermal evaporation at a temperature of approximately 1500°C with a current of 50 A through the crucible. The aerosol population produced under these conditions was very stable with variations of less than 5% in concentration at any given RDMA voltage. In Fig. 5(a) we show how the electrometer current changes as a function of the magnitude of the RDMA voltage (for $V_{RDMA} < 0$) when the aerosol is run through the neutralizer as well as when the neutralizer is bypassed. Fig. 5(b) reveals the effect of polarity reversal in the RDMA voltage for an aerosol that has bypassed the neutralizer.

When $V_{RDMA} < 0$ and the aerosol is run through the neutralizer as in Fig. 5(a), a typical log-normal relationship centered around 2400 V is obtained between electrometer current and analyzer voltage. Furthermore, no current was detected at the electrometer for $V_{RDMA} = 0$, suggesting that for these experimental conditions the excessive concentration of negative particles was not sufficient to induce a significant space-charge field. When the aerosol is forced to bypass the neutralizer, an apparent shift of the data points toward higher voltages is observed, with the log-normal-type relationship now centered around 3300 V. Several causes could be responsible for this observation and caution must be exercised in comparing measurements made with and without the neutralizer. The absence of the neutralizer leads to different aerosol residence time and charge state. These may affect Brownian coagulation and diffusion losses of a high-concentration aerosol which in turn may cause changes in the aerosol number concentration and mobility distribution. It is possible, however, that a significant space-charge field exists in the RDMA now

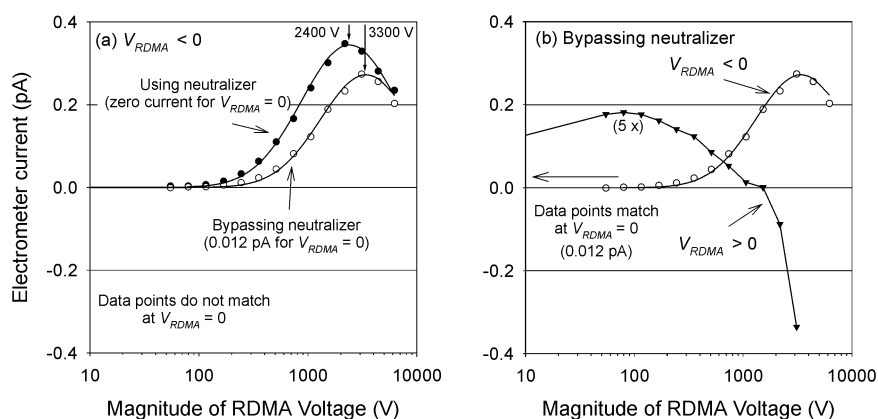


Fig. 5. Electrometer current as a function of the magnitude of the applied voltage in an experiment using the thermal evaporation source. (a) Effect of bypassing the neutralizer when $V_{RDMA} < 0$ and (b) effect of polarity reversal for an aerosol that has bypassed the neutralizer. The traces in part (a) are log-normal fits to the data points.

that the aerosol no longer has an equilibrium bipolar charge distribution. Evidence that this might be the case is that for this condition, a positive current (0.012 pA) was detected by the electrometer for $V_{\text{RDMA}} = 0$. Once again the field generated by the particle cloud might be forcing particles to migrate across the sheath flow and be extracted in the absence of an applied voltage. The same field could add to the applied electric field leading to a shift of the mobility distribution toward higher voltages.

The most interesting phenomenon, however, occurs when the field polarity is reversed in the RDMA ($V_{\text{RDMA}} > 0$) and an aerosol that bypassed the neutralizer is analyzed. This is shown in Fig. 5(b). As one steps through voltage, positively charged particles are sampled, and the aerosol concentration climbs slowly up to a voltage of ~ 100 V, dropping to zero above ~ 1000 V. As the voltage continues to rise, particles with the opposite polarity begin to be sampled out of the instrument.

This suggests the presence of a significant space-charge field in the RDMA that causes positive particles to migrate across the sheath flow when the applied voltage is zero. By increasing the voltage, a point is reached when the space-charge field is balanced and the positively charged particles are driven away from the sampling outlet. For higher voltages still, the applied field totally overcomes the space-charge field causing negatively charged particles to be sampled. The high electric fields required to bring the electrometer current down to zero (100–1000 V/cm) indicate that if this phenomenon is indeed related to a space-charge field in the RDMA, a highly charged aerosol is present in the instrument. The concentration of singly charged particles necessary to generate a space-charge field of this magnitude is in the 10^{10} – 10^{11} cm^{-3} range. These high concentrations are not consistent with the residence time of our experimental setup (~ 10 s) which sets an upper limit on the total number concentration between 10^8 and 10^9 cm^{-3} due to Brownian coagulation. Thus, in this case most of the aerosol charge must be associated with multiply charged particles as the neutralizer was bypassed in this measurement and the thermal evaporation process is expected to induce multiple charging.

In order to see how much the mobility classification was being affected during these measurements, we have collected particles at the hypersonic impactor and analyzed them by TEM. Fig. 6(a) shows a micrograph of silicon particles generated by spark discharge under the same conditions of Fig. 4 (aerosol run through the neutralizer). A voltage of -16 V was used on the RDMA (corresponding to 4-nm singly charged particles). The image shows a surprisingly polydisperse population, ranging from isolated particles with diameter around 10 nm to agglomerates as large as 60 nm. Measurements of the projected-area equivalent diameter on this image yield the histogram of Fig. 6(b). For comparison, Fig. 6(b) also shows the diffusion-broadened RDMA transfer function as obtained from previous tandem DMA measurements (Zhang & Flagan, 1996) and deposits of classified particles (Camata et al., 1996) when space-charge effects were decisively ruled out.² The shift and broadening of the size distribution on the TEM image with respect to the calibration curves indicate that the mobility classification was severely compromised.

² As seen in Fig. 6(b), the RDMA transfer function estimated by TEM on deposits of classified particles is significantly broader than the one obtained from tandem DMA measurements. This is most likely a result of the low-particle statistics on the samples analyzed by TEM as well as flow instabilities over the long periods of particle deposition required to generate those samples.

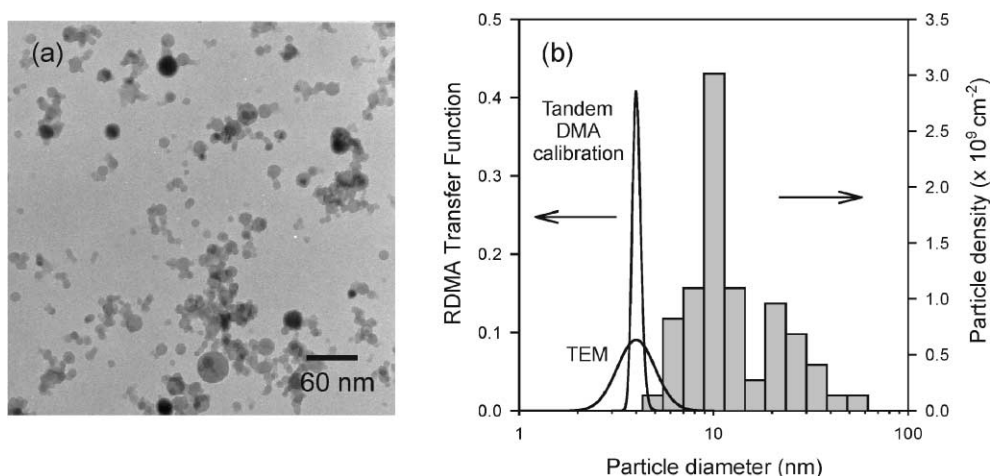


Fig. 6. (a) Transmission electron microscopy image of silicon particles generated by spark discharge, run through the neutralizer and collected on a carbon substrate by hypersonic impaction after mobility classification. The voltage on the analyzer was -16 V, corresponding to a diameter of 4 nm for singly charge particles. (b) Size distribution obtained from the image (histogram). The solid lines indicate, for comparison, the RDMA transfer function as determined from tandem DMA calibration measurements (Zhang & Flagan, 1996) and from transmission electron microscopy (TEM) experiments (Camata et al., 1996).

Although qualitative in nature, these measurements show that space-charge effects may become severe in the processing of highly charged aerosols. They illustrate that if the DMA is to be used effectively as a processing device in similar situations, this kind of distortion must be avoided.

As an attempt to gain some understanding of the phenomenon and improve the DMA performance in the regime of interest, we discuss in the next section the effect of the DMA design parameters and operation conditions on the intensity of the space-charge field.

4. Estimating the intensity of the space-charge effect

The presence of a non-negligible space-charge field affects the particle trajectories in the DMA. In principle, the trajectory of a particle of mobility Z_p^* may be found from the equations of motion

$$\begin{aligned}\frac{dr}{dt} &= u_r + Z_p^*(E_r^{ap} + E_r^{sc}), \\ \frac{dz}{dt} &= u_z + Z_p^*(E_z^{ap} + E_z^{sc}),\end{aligned}\quad (2)$$

where r and z denote the radial and axial coordinates, u_r and u_z are the components of the gas-flow velocity, E_r^{ap} and E_z^{ap} represent the applied electric field, while E_r^{sc} and E_z^{sc} are the components of the space-charge field. The space-charge field may, in principle, be calculated using Poisson's equation

$$\nabla^2\phi(r, z) = -\frac{\rho(r, z)}{\varepsilon}\quad (3)$$

with

$$\mathbf{E}^{\text{sc}}(r, z) = -\nabla\phi(r, z). \quad (4)$$

The complexity associated with a thorough solution of this problem is evident. The charge density $\rho(r, z)$ depends on the details of the particle trajectories which in turn depend on $\rho(r, z)$ via the space-charge field. A detailed calculation of the DMA transfer function including the space-charge field is thus a complex problem.

Without attempting a full solution of this problem, we will instead introduce a dimensionless group that roughly estimates the importance of the space-charge field. Although this dimensionless group will not capture the details of the physical phenomenon involved, its scaling provides the essential features of the process and can be useful in the design of DMAs tailored for operation at high concentration of charged particles.

In order to make our approach somewhat general, we will keep the two most common DMA geometries in mind, namely, the radial DMA (RDMA) and the cylindrical DMA (CDMA).

Let us consider a DMA operating with an applied voltage V and flow rates Q_a (aerosol), Q_{sh} (sheath), Q_s (sample) and Q_e (excess). The particles that enter the analyzer through the aerosol inlet are initially confined to a boundary layer of width δ . Assuming plug flow, the thickness of this boundary layer in the RDMA can be written as

$$\delta = \left(\frac{\beta}{1 + \beta}\right)b, \quad (5)$$

where

$$\beta = \frac{Q_a + Q_s}{Q_{\text{sh}} + Q_e} \quad (6)$$

and b is the distance between the RDMA electrodes. For the CDMA the same plug flow assumption leads to

$$\delta = r_2 - \sqrt{\frac{\beta}{1 + \beta} \left(r_1^2 + \frac{1}{\beta}r_2^2\right)}, \quad (7)$$

where r_1 and r_2 represent the diameters of the inner and outer electrodes of the CDMA, respectively.

Let us assume further that we have a unipolar aerosol with concentration N containing only singly charged particles. For the RDMA, we may then write the charge density close to the aerosol inlet in terms of the axial coordinate z as

$$\rho(z) = \begin{cases} Ne, & b - \delta < z < b, \\ 0 & \text{otherwise,} \end{cases} \quad (8)$$

where e is the elementary charge. For the CDMA, this charge density becomes a function of the radial coordinate r and may be expressed as

$$\rho(r) = \begin{cases} Ne, & r_a < r < r_2, \\ 0 & \text{otherwise,} \end{cases} \quad (9)$$

where

$$r_a \equiv r_2 - \delta = \sqrt{\frac{\beta}{1 + \beta} \left(r_1^2 + \frac{1}{\beta} r_2^2 \right)}.$$

The charge densities of Eqs. (8) and (9) are true only in a region arbitrarily close to the DMA aerosol inlet, where migration and Brownian diffusion are still negligible. For a unipolar aerosol, this is the region where the space-charge field is strongest, as the aerosol concentration is the highest. Let us then use these simple expressions to obtain a rough estimate of the intensity of the space-charge field at this location. In both geometries the solution of this problem can be found at once by solving a one-dimensional Poisson's equation. For the RDMA this equation takes the form

$$\frac{\partial^2 \phi(z)}{\partial z^2} = -\frac{\rho(z)}{\varepsilon} \quad (10)$$

with $\rho(z)$ given by Eq. (8). For the CDMA, Poisson's equation is written as

$$\frac{1}{r} \frac{\partial}{\partial r} \left(r \frac{\partial \phi(r)}{\partial r} \right) = -\frac{\rho(r)}{\varepsilon} \quad (11)$$

with $\rho(r)$ given by Eq. (9). Integrating twice and imposing boundary conditions, Eqs. (10) and (11) yield the electric potential near the aerosol inlet of the RDMA and the CDMA. Using the definition

$$\mathbf{E} = -\nabla \phi \quad (12)$$

the electric field is promptly calculated. Therefore, the electric field in the particle-free region near the aerosol inlet of both instruments is found to be

$$E_z^{\text{RDMA}} = \frac{V}{b} \left(1 + \frac{Ne}{\varepsilon V} G_F \right) \quad (13)$$

and

$$E_r(r)^{\text{CDMA}} = \frac{V}{\ln(r_2/r_1)} \frac{1}{r} \left(1 + \frac{Ne}{\varepsilon V} G_F \right), \quad (14)$$

where G_F is a factor that depends on the flow rates and the geometry of the DMA.

Eqs. (13) and (14) were conveniently arranged to show that, for both the RDMA and the CDMA, the applied electric field (quantity outside the parentheses) is modified by a dimensionless group that depends on the concentration of singly charged particles N , the applied voltage V , and the flow rates and the geometry of the DMA, G_F . We will call this dimensionless group the *space-charge number*, Sc , which we write as

$$Sc \equiv \frac{Ne}{\varepsilon V} G_F. \quad (15)$$

For the RDMA the factor G_F takes the form

$$G_F^{\text{RDMA}} = \frac{1}{2} \left(\frac{\beta}{1 + \beta} \right)^2 b^2 \quad (16)$$

while for the CDMA G_F is

$$G_F^{\text{CDMA}} = \frac{1}{4} r_2^2 \left\{ 1 - \left(\frac{r_a}{r_2} \right)^2 \left[1 - \ln \left(\frac{r_a}{r_2} \right)^2 \right] \right\} \quad (17)$$

The annular gap of the CDMA looks like the parallel plates of the RDMA when its width is small compared to the radius. Thus, it can be shown that G_F^{CDMA} approaches the value of G_F^{RDMA} when $(r_2 - r_1)/r_2 \rightarrow 0$, i.e.

$$\lim_{r_1/r_2 \rightarrow 1} G_F^{\text{CDMA}} = G_F^{\text{RDMA}}. \quad (18)$$

Although derived for simplified space-charge conditions (near the aerosol inlet), the space-charge number defined by Eq. (15) can provide rough estimates of the importance of the space-charge effect in a DMA under given operating conditions. Its value can be interpreted simply as an estimate of the ratio of the space-charge field strength to the applied electric field. The dependence of the space-charge number with number concentration of singly charged particles is shown in Fig. 7 for different applied voltages, electrode separations and DMA geometries.

Fig. 7(a) shows the effect of applied voltage on the space-charge number for two electrode separations in the RDMA. The most dramatic distortions are expected when low applied voltages and large electrode separations are used. At 1 V and $b = 1$ cm, for example, a field alteration of as much as 75% is predicted for $N = 10^8 \text{ cm}^{-3}$. Increased applied voltages and reduced electrode separations diminish the relative importance of the space-charge by strengthening the applied electric field and reducing the width of the charged aerosol stream. This can be seen in a straightforward manner for the RDMA if one considers the expression for Sc (Eqs. (15) and (16)). It is evident that

$$\text{Sc}^{\text{RDMA}} \propto \frac{b^2}{V} = \frac{b}{E_z^{\text{ap}}}, \quad (19)$$

where E_z^{ap} is the applied electric field. The space-charge effect is minimized by simultaneously maximizing the applied electric field and minimizing the electrode separation. It is interesting to note that the minimization of the electrode separation b plays a dual role in minimizing Sc. It leads to an increase in the applied electric field ($E_z^{\text{ap}} = V/b$) while reducing at the same time the width of the aerosol boundary layer, which results in further reduction of the space-charge effect. The same trend is also true for the CDMA design.

Fig. 7(a) also indicates why space-charge effects can usually be ignored in DMA studies. It turns out that the field distortions are negligible for number concentrations below 10^5 cm^{-3} and particle size above 10 nm (applied voltages in excess of 100 V), which is the regime where traditionally most DMA studies are performed. However, as DMAs are applied to high-concentration aerosol processing of particles as small as 1 nm, space-charge distortions have to be taken into account or limited by the proper choice of applied voltage and geometry.

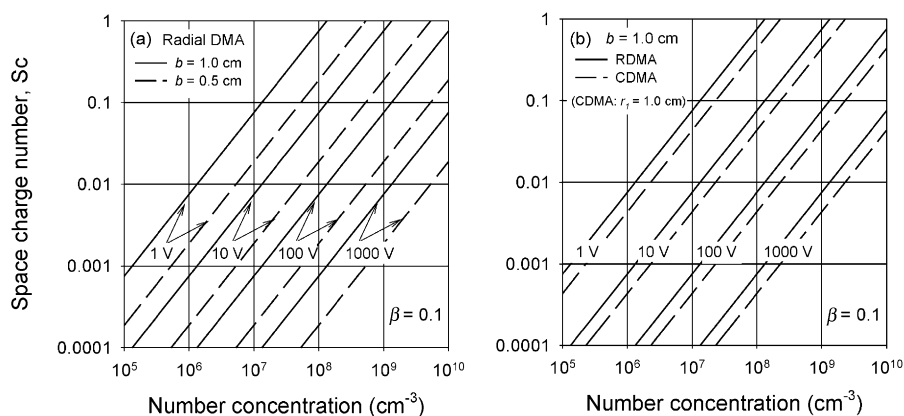


Fig. 7. (a) Dependence of the space-charge number with total number concentration for different electrode separations in the radial DMA. (b) Comparison between the space-charge number for the radial DMA (RDMA) and the cylindrical DMA (CDMA) for an electrode separation of 1 cm and CDMA inner electrode radius $r_1 = 1$ cm.

In Fig. 7(b) we present a comparison between the space-charge number for a RDMA with $b = 1$ cm and a CDMA with $r_2 - r_1 = 1$ cm ($r_1 = 1$ cm). The figure reveals that for this particular choice of r_1 and electrode separation, the CDMA has an advantage over the radial design for reducing space-charge effects. The space-charge number for the CDMA is about 42% less than the value predicted for the RDMA.

5. Toward a DMA for high-throughput nanoparticle processing

A DMA for materials processing has to be designed to handle large concentrations of charged particles. Based on the simple analysis discussed here, it becomes apparent that the critical parameters that should be optimized to limit space-charge distortions are the applied electric field and the electrode separation. A DMA designed to operate at the maximum possible applied electric field with the minimum possible electrode separation will minimize space-charge effects and enable reliable classification at high concentrations.

Maximizing the applied electric field also minimizes diffusion broadening of the DMA transfer function. This can be seen by examining the ratio of electrophoretic migration to diffusive transport, a quantity known as the Peclet number for particle migration (Zhang & Flagan, 1996)

$$\text{Pe}_{\text{mig}} = \frac{v_{\text{E}}^* b}{\mathcal{D}}, \quad (20)$$

where v_{E}^* is the particle migration velocity, b is the migration path length, i.e., the distance between the DMA electrodes, and \mathcal{D} is the particle diffusion coefficient. For the RDMA v_{E}^* is given by

$$v_{\text{E}}^* = Z_{\text{p}}^* E_z^{\text{ap}} = Z_{\text{p}}^* \frac{V}{b} = \frac{q \mathcal{D} V}{kT}, \quad (21)$$

where q is the charge on the particle and V is the applied voltage. The migration Peclet number thus becomes

$$\text{Pe}_{\text{mig}}^{\text{RDMA}} = \frac{qV}{kT}. \quad (22)$$

For the CDMA, the electric field and migration velocity vary with radial position, i.e.

$$v_{\text{E}}^* = Z_{\text{p}}^* E_{\text{r}}^{\text{ap}} = \frac{q\mathcal{D}V}{kT \ln(r_2/r_1)} \frac{1}{r} \quad (23)$$

and $b = r_2 - r_1$. Expressing the migration Peclet number in terms of the migration velocity at the outer cylinder yields

$$\text{Pe}_{\text{mig}}^{\text{CDMA}} = \frac{qV}{kT} \frac{r_2 - r_1}{\ln(r_2/r_1)} \frac{1}{r_2}. \quad (24)$$

Eqs. (22) and (24) reveal that for both the RDMA and the CDMA, Pe_{mig} is proportional to qV/kT , i.e., the ratio of the electrostatic potential energy of the migrating particle to its thermal energy. Maximizing the voltage leads to maximized electrostatic energy and the importance of thermal effects such as diffusion is minimized (Flagan, 1999). Hence, a DMA that is designed to operate at the maximum possible applied electric field will contribute not only to the minimization of space-charge effects but also diffusion effects.

Commonly available DMAs are not designed to operate at high electric fields in the classification of particles below 10 nm because that implies a severe limitation in their dynamic range. However, for the specific purpose of nanoparticle processing in the 1–10 nm range at high concentrations, the DMA design can be optimized to allow high-resolution performance in the size and concentration range of interest if a limited dynamic range is acceptable.

6. Summary

In general, DMAs are operated at typical charged particle number concentrations well below 10^5 cm^{-3} . These concentrations are consistent with the study of dilute systems that seek to elucidate the dynamics of aerosol populations. Today's condensation nucleus counters have enabled single particle detection down to 3 nm and low concentrations are usually preferred as they are known to avoid space-charge effects in the DMA. For materials synthesis by nanoparticle processing, however, the operation at high number concentration of charged particles is unavoidable. It is often imperative the production of dense deposits containing *milligrams* of mobility classified particles, which can only be achieved in reasonable times and flow rates if number concentrations of charged particles well above 10^5 cm^{-3} are utilized.

We have observed that operation at these conditions may lead to a breakdown in mobility classification in the radial DMA. Estimates based on a simple dimensionless group, the space-charge number, show that the applied electric field and the electrode separation are the crucial parameters in minimizing space-charge effects. Analyzers designed to operate at high electric fields

and small electrode separations are the ones to achieve minimum space-charge distortions at elevated number concentrations. This design strategy also leads to minimized diffusion broadening of the DMA transfer function. Hence, instruments developed according to this rationale will be compatible with the high-throughput and high-resolution requirements necessary for materials synthesis based on nanoparticle processing.

Acknowledgements

This work was supported by the US National Science Foundation under Grant NSF-DMR-98-71850. R.P.C. acknowledges support from CNPq, Brasília, Brazil. The authors would like to thank Dr. Gang He and Prof. Kerry J. Vahala for valuable discussions.

References

- Adachi, M., Kousaka, Y., & Okuyama, K. (1985). Unipolar and bipolar diffusion charging of ultrafine aerosol particles. *Journal of Aerosol Science*, *16*, 109–123.
- Alonso, M., & Kousaka, Y. (1996). Mobility shifts in the differential mobility analyzer due to Brownian diffusion and space-charge effects. *Journal of Aerosol Science*, *27*, 1201–1225.
- Camata, R.P., Atwater, H.A., Vahala, K.J., & Flagan, R.C. (1996). Size classification of silicon nanocrystals. *Applied Physics Letters*, *68*, 3162–3164.
- Chen, D.-R., & Pui, D.Y.H. (1997). Numerical modeling of the performance of differential mobility analyzers for nanometer aerosol measurements. *Journal of Aerosol Science*, *28*, 985–1004.
- Chen, D.-R., & Pui, D.Y.H. (1998). A novel charger for nanometer aerosols. *Journal of Aerosol Science*, *29*, S1023–S1024.
- Chen, D.-R., Pui, D.Y.H., Hummes, D., Fissan, H., Quant, F.R., & Sem, G.J. (1998). Design and evaluation of a nanometer aerosol differential mobility analyzer (Nano-DMA). *Journal of Aerosol Science*, *29*, 497–509.
- Chen, D.-R., Pui, D.Y.H., Mulholland, G.W., & Fernandez, M. (1999). Design and testing of an aerosol sheath inlet for high resolution measurements with a DMA. *Journal of Aerosol Science*, *30*, 983–999.
- Dinh, L.N., Chase, L.L., Balooch, M., Siekhaus, W.J., & Wooten, F. (1996). Optical properties of passivated Si nanocrystals and SiO_x nanostructures. *Physical Review B*, *54*, 5029–5037.
- Eichler, L., de Juan, L., & Fernández de la Mora, J. (1998). Improvement of the resolution of TSI's 3071 DMA via redesigned sheath air and aerosol inlets. *Aerosol Science and Technology*, *29*, 39–49.
- Fernández de la Mora, J., Hering, S.V., Rao, N., & McMurry, P.H. (1990). Hypersonic impaction of ultrafine particles. *Journal of Aerosol Science*, *21*, 169–187.
- Flagan, R.C. (1998). History of Electrical Aerosol Measurements. *Aerosol Science and Technology*, *28*, 301–380.
- Flagan, R.C. (1999). On differential mobility analyzer resolution. *Aerosol Science and Technology*, *30*, 556–570.
- Knutson, E. O., & Whitby, K. T. (1975). Aerosol classification by electric mobility: Apparatus, theory, and applications. *Journal of Aerosol Science*, *6*, 453–460.
- Kousaka, Y., Okuyama, K., Adachi, M., & Mimura, T. (1986). Effect of Brownian diffusion on electrical classification of ultrafine aerosol particles in differential mobility analyzer. *Journal of Chemical Engineering of Japan*, *19*, 401–407.
- Kruis, F.E., Fissan, H., & Peled, A. (1998a). Synthesis of nanoparticles in the gas phase for electronic, optical and magnetic applications — a review. *Journal of Aerosol Science*, *29*, 511–535.
- Kruis, F.E., Otten, F., Jordan, F., & Fissan, H. (1998b). A new efficient unipolar charger for nanoparticles. *Journal of Aerosol Science*, *29*, S1021–S1022.
- Magnusson, M.H., Deppert, & Krinke, T. (1998). Thermal charging of metal nanoparticles. *Journal of Aerosol Science*, *29*, S847.
- Magnusson, M.H., Deppert, K., Malm, J.-O., & Svensson, C. (1997). Size-selected GaN and InN nanocrystals. *Journal of Aerosol Science*, *28*, S471.

- Mesbah, B. (1994) *Le Spectrometre de mobilite electrique circulaire: theorie, performances et applications*. Ph.D. thesis, University of Paris.
- Saunders, W.A., Sercel, P.C., Lee, R.B., Atwater, H.A., Vahala, K.J., Flagan, R.C., & Escorcia-Aparcio, E. J. (1993). Synthesis of luminescent silicon clusters by spark ablation. *Applied Physics Letters*, 63, 1549–1551.
- Schwing, S., Garwin, E., & Schmidt-Ott, A. (1988). Aerosol generation by spark discharge. *Journal of Aerosol Science*, 19, 639–642.
- Stolzenburg, M.R. (1988). *An ultrafine aerosol size distribution measuring system*. Ph.D. thesis, University of Minnesota.
- Tammet, H.F. (1970). *The aspiration method for the determination of atmospheric-ion spectra*. Israel Program for Scientific Translations, Jerusalem (The original work in Russian was published in 1967).
- Winklmayr, W., Reischl, G.P., Lidner, A.O., & Berner, A. (1991). A new electro-mobility spectrometer for the measurement of aerosol size distributions in the size range from 1 to 1000 nm. *Journal of Aerosol Science*, 22, 289–296.
- Yun, S.-M, Otani, Y., & Emi, H. (1997). Development of Unipolar Ion Generator-Separation of Ions in Axial Direction of Flow. *Aerosol Science and Technology*, 26, 389–397.
- Zhang, S.-H., Akutsu, Y., Russell, L.M., Flagan, R.C., & Seinfeld, J. H. (1995). Radial differential mobility analyzer. *Aerosol Science and Technology*, 23, 357–372.
- Zhang, S.-H., & Flagan, R.C. (1996). Resolution of the radial differential mobility analyzer. *Journal of Aerosol Science*, 27, 1179–1200.